Eur. Phys. J. B **68**, 353–364 (2009)
DOI: 10.1140/epjb/e2008-00463-7

THE EUROPEAN PHYSICAL JOURNAL B

Regular Article

Quantum diffusion of matter waves in 2D speckle potentials

C. Miniatura[1,4,5], R.C. Kuhn[2,4], D. Delande[3], and C.A. Müller[2,a]

[1] Institut Non Linéaire de Nice, UMR 6618, Université de Nice Sophia, CNRS; 1361 route des Lucioles, 06560 Valbonne, France
[2] Physikalisches Institut, Universität Bayreuth, 95440 Bayreuth, Germany
[3] Laboratoire Kastler-Brossel, Université Pierre et Marie Curie-Paris 6, ENS, CNRS; 4 Place Jussieu, 75005 Paris, France
[4] Centre for Quantum Technologies, National University of Singapore, 3 Science Drive 2, 117543 Singapore, Singapore
[5] IPAL, CNRS, I2R; 1 Fusionopolis Way, 138632 Singapore, Singapore

Received 23 July 2008 / Received in final form 28 October 2008
Published online 24 December 2008 –

Abstract. This paper investigates quantum diffusion of matter waves in two-dimensional random potentials, focussing on expanding Bose-Einstein condensates in spatially correlated optical speckle potentials. Special care is taken to describe the effect of dephasing, finite system size, and an initial momentum distribution. We derive general expressions for the interference-renormalized diffusion constant, the disorder-averaged probability density distribution, the variance of the expanding atomic cloud, and the localized fraction of atoms. These quantities are studied in detail for the special case of an inverted-parabola momentum distribution as obtained from an expanding condensate in the Thomas-Fermi regime. Lastly, we derive quantitative criteria for the unambiguous observation of localization effects in a possible 2D experiment.

PACS. 03.75.Kk Dynamic properties of condensates; collective and hydrodynamic excitations, superfluid flow – 42.25.Dd Wave propagation in random media – 72.15.Rn Localization effects

1 Introduction

In recent years an increasing number of theoretical and experimental studies discussed the transport of ultra-cold atoms and Bose-Einstein condensates in the presence of disorder [1] (and references therein). One emblematic phenomenon in the field is the celebrated Anderson localization phenomenon, a disorder-induced metal-insulator transition observed in the absence of inter-particle interactions [2–4]. Recently two papers have reported experimental evidence for exponential spatial localization of matter waves using dilute Bose-Einstein condensates in a 1D optical speckle potential [5] and in a quasi-periodic optical lattice [6]. These results call for investigations in higher dimensions as it is known that transport in disordered 1D and 2D potentials always occurs in the localized regime whereas in 3D there is a transition [7].

In two preceding articles [8,9] we presented a theoretical description for the quantum diffusion of monochromatic non-interacting ultra-cold atoms in 2D and 3D disordered optical potentials. In real experiments, a crucial question in this context is the influence of a finite initial momentum distribution of the atoms, together with the limits imposed by dephasing processes, like spontaneous emission, and boundaries. These questions are addressed in the present paper, focussing on the case of 2D optical speckle potentials. Coherent diffusive transport of non-interacting matter waves is studied for any initial Wigner phase-space distribution within the framework of the self-consistent theory of localization [9–11]. Within this formalism, we then analyze the influence of dephasing processes and of boundaries. The expected diffusion constant is calculated, both for the momentum distribution of an interaction-driven expansion of a Bose-Einstein condensate [12] and a Gaussian momentum distribution [13]. Finally, we derive criteria for the experimental observation of Anderson localization in 2D correlated speckle potentials.

The paper is structured as follows: we first recall in Section 2 some basics about propagation in disordered systems and calculate the expected probability density distribution and the variance of the expanding cloud. As a first application, we discuss the case of phase-incoherent, classical diffusion in Section 3. Section 4 considers coherent corrections to transport, viz., weak and strong localization. We calculate the diffusion constant self-consistently at finite frequency. In the stationary limit, this leads to the shape of the localized density distribution and the relevant localization length. In Section 5, we incorporate the effect of dephasing by spontaneous emission into the formalism, and derive criteria for the effective threshold separating the diffusive from the (almost) localized regime, where only very slow residual diffusion occurs. Sections 6

[a] e-mail: cord.mueller@uni-bayreuth.de

and 7 are devoted to the implications of finite system size and experimental realizability.

2 Transport in disordered systems

In this paper we describe the dynamics of non-interacting cold atomic gases evolving in static two-dimensional random potentials $V(\boldsymbol{r})$. If interaction plays no role, a one-body description of the atomic dynamics is justified. The quantum dynamics is then described by the Hamiltonian

$$H = \frac{p^2}{2m} + V(\boldsymbol{r}), \tag{1}$$

where $V(\boldsymbol{r})$ describes the potential fluctuations around its average value, which we choose to be the origin of energies. In a single realization of the disorder, an initial plane wave $\boldsymbol{k}$ with kinetic energy $E_k = \hbar^2 k^2/(2m)$ will be randomly scattered by the potential fluctuations to all other accessible states. As a consequence, only statistical quantities obtained by configuration average over the disorder realizations can reveal generic transport properties. In the following, configuration averages will be denoted by $\overline{(\ldots)}$, and as a first property of the disorder potential, $\overline{V(\boldsymbol{r})} = 0$.

2.1 Spatial potential correlations

Experimentally, random potentials $V(\boldsymbol{r})$ can be realized as optical speckle potentials generated by monochromatic illumination and imaging of an appropriate diffusing plate [14]. In the regime of parameters that we will explore, the pair correlation $\overline{V(\boldsymbol{r}+\boldsymbol{r}')V(\boldsymbol{r}')}$ is the only ingredient one needs to calculate relevant microscopic quantities characterizing the atomic dynamics [9]. The potential fluctuations are then characterized by the pair correlation

$$\overline{V(\boldsymbol{r}+\boldsymbol{r}')V(\boldsymbol{r}')} = V^2 C(r/\zeta) \tag{2}$$

that depends only on the modulus $r = |\boldsymbol{r}|$ when translation and rotation invariance is restored on average. The spatial correlation function $C(\rho = r/\zeta)$ decays from $C(0) = 1$ to zero over a characteristic spatial scale ζ. In the case of an optical speckle potential this correlation length $\zeta_{\rm opt} = (\alpha k_L)^{-1}$ is set by the wavelength $\lambda_L = 2\pi/k_L$ of the monochromatic laser field and by the numerical aperture α of the imaging system (in current experiments $\alpha \sim 0.3$).

A 2D optical speckle potential created from a circular diffusive plate is described by [9,15]

$$C_{\rm opt}(\rho) = (2J_1(\rho)/\rho)^2 \tag{3}$$

where $J_1(\rho)$ is the Bessel function of order 1. Its 2D Fourier transform $P(\boldsymbol{\kappa}) = \int d\boldsymbol{\rho}\, e^{-i\boldsymbol{\kappa}\cdot\boldsymbol{\rho}} C(\rho)$, also known as the fluctuation power spectrum, is given by

$$P_{\rm opt}(\boldsymbol{\kappa}) = 8\left[\arccos\tfrac{\kappa}{2} - \tfrac{\kappa}{2}\sqrt{1-(\tfrac{\kappa}{2})^2}\right]\Theta(2-\kappa). \tag{4}$$

The slow algebraic decay of the real-space correlations (as ρ^{-3}) implies that their Fourier transform is non-analytic at $\kappa = 0$: $P_{\rm opt}(\boldsymbol{\kappa}) = 4\pi - 4|\boldsymbol{\kappa}| + O(\kappa^2)$. Also the fact that the power spectrum has finite support in k-space has important consequences for the localization of matter waves in a 1D geometry, allowing for the crossover from exponential to effectively algebraic localization in position space [5,12].

Potential correlations are also often described (or approximated) by a Gaussian correlator, such as in [16], because it is easily implemented in the numerics and leads to somewhat simpler analytical calculations:

$$C_{\rm gauss}(\rho) = \exp\left(-\rho^2/2\right), \tag{5a}$$

$$P_{\rm gauss}(\kappa) = (2\pi)^{d/2}\exp\left(-\kappa^2/2\right). \tag{5b}$$

If one wishes to match the small-$\boldsymbol{r}$ expansion of the 2D optical speckle (3) one must choose $\zeta_{\rm gauss} = \sqrt{2}\zeta_{\rm opt}$. The power spectrum (5b) decays as a Gaussian, which is often a qualitatively good approximation to the finite support of the true optical speckle spectrum (4).

If only the behavior at very low momenta $\kappa = k\zeta \ll 1$ is of interest, the detailed structure of the correlation function is unimportant, and a good and simple approximation is provided by $P(\kappa) \approx P(0)$ where $P_{\rm opt}(0) = 4\pi$ and $P_{\rm gauss}(0) = (2\pi)^{d/2}$. This in turn corresponds to an effectively δ-correlated position-space correlator

$$\overline{V(\boldsymbol{r}+\boldsymbol{r}')V(\boldsymbol{r}')} = V^2 P(0)\zeta^d \delta(\boldsymbol{r}). \tag{6}$$

2.2 Weak disorder regime

The correlation length ζ defines a correlation energy

$$E_\zeta = \frac{\hbar^2}{m\zeta^2} \tag{7}$$

and its associated time scale $\tau_\zeta = \hbar/E_\zeta = m\zeta^2/\hbar$. The matter wave dynamics is then driven by three different energy scales: the kinetic energy E_k, the strength V of potential fluctuations, and the correlation energy E_ζ.

The impact of potential fluctuations on the atomic dynamics is simply estimated by the magnitude $V\tau/\hbar$ of the random phase kick experienced by an atom travelling over the distance $\zeta = v\tau$ at velocity $v = \hbar k/m$ through potential fluctuations of strength V. As shown in [9], the weak-scattering regime is realized if

$$\frac{V\tau}{\hbar} = \sqrt{\frac{E_\Delta}{2E_k}} = \frac{\eta}{k\zeta} \ll 1. \tag{8}$$

Throughout the paper, we will use

$$\eta = \frac{V}{E_\zeta} \tag{9}$$

as a measure for the potential fluctuation strength. Condition (8) shows that the weak-disorder regime is realized if the kinetic energy E_k is sufficiently above the important energy scale $E_\Delta = V^2/E_\zeta$. In 3D, this is essentially the mobility edge separating extended states with $E_k > E_\Delta$ from localized ones with $E_k < E_\Delta$ [9].

Even within the weak scattering regime $E_k \gg E_\Delta$ one may still be able to probe the low-energy or δ-correlated potential regime $E_k \ll E_\zeta$ provided the following energy hierarchy holds: $E_\Delta \ll E_k \ll E_\zeta$. This requires very weak potential fluctuations $V \ll E_\zeta$ or equivalently $\eta \ll 1$.

In the weak-scattering regime the atoms experience thus many random phase kicks of small amplitude in the course of time, which repeatedly alter their wave function. These phase kicks are the seeds of a diffusive behavior for the average probability density that will be calculated in the following.

2.3 Phase-space dynamics

The ensemble-averaged atomic dynamics in a d-dimensional potential is fully described by the average Wigner distribution [17]:

$$W_t(\boldsymbol{r},\boldsymbol{k}) = \int d\boldsymbol{r}'\, e^{-i\boldsymbol{k}\cdot\boldsymbol{r}'} \left\langle \boldsymbol{r} + \tfrac{\boldsymbol{r}'}{2} | \overline{\varrho(t)} | \boldsymbol{r} - \tfrac{\boldsymbol{r}'}{2} \right\rangle \tag{10}$$

where $\overline{\varrho(t)} = \overline{U(t)\,\varrho_0\,U^\dagger(t)}$ is the one-particle average density operator. Here ϱ_0 denotes the initial atomic density operator and $U(t) = \Theta(t)\exp\{-iHt/\hbar\}$ is the forward-time evolution operator for the Hamiltonian (1), Θ being the Heaviside step function. From this Wigner function one can extract the marginals $p(\boldsymbol{r},t)$ (spatial distribution at time t) and $\pi(\boldsymbol{k},t)$ (momentum distribution at time t) according to:

$$p(\boldsymbol{r},t) = \int \frac{d\boldsymbol{k}}{(2\pi)^d}\, W_t(\boldsymbol{r},\boldsymbol{k}), \quad \pi(\boldsymbol{k},t) = \int d\boldsymbol{r}\; W_t(\boldsymbol{r},\boldsymbol{k}). \tag{11}$$

The normalization of these marginals is

$$\int \frac{d\boldsymbol{k}}{(2\pi)^d}\, \pi(\boldsymbol{k},t) = \int d\boldsymbol{r}\; p(\boldsymbol{r},t) = 1, \tag{12}$$

which means that the Wigner distribution W_t is normalized as

$$\int \frac{d\boldsymbol{r}d\boldsymbol{k}}{(2\pi)^d}\, W_t(\boldsymbol{r},\boldsymbol{k}) = 1. \tag{13}$$

Rewriting the integrand of (10) by separating the initial Wigner distribution W_0 gives W_t in the form

$$W_t(\boldsymbol{r},\boldsymbol{k}) = \int \frac{d\boldsymbol{r}'d\boldsymbol{k}'}{(2\pi)^d}\, G_t(\boldsymbol{r},\boldsymbol{k};\boldsymbol{r}',\boldsymbol{k}')\, W_0(\boldsymbol{r}',\boldsymbol{k}') \tag{14}$$

with a rather transparent physical meaning: starting from the point $(\boldsymbol{r}',\boldsymbol{k}')$ at time $t=0$, the initial quasi-probability W_0 is propagated in phase space with G_t to give W_t. The phase-space propagation kernel G_t thus encapsulates the relevant quantum dynamics and reads:

$$G_t = \int d\boldsymbol{r}_1 d\boldsymbol{r}_2\, e^{-i(\boldsymbol{k}\cdot\boldsymbol{r}_1 - \boldsymbol{k}'\cdot\boldsymbol{r}_2)}\, \mathcal{L}_t(\boldsymbol{r},\boldsymbol{r}',\boldsymbol{r}_1,\boldsymbol{r}_2) \tag{15a}$$

$$\mathcal{L}_t = \overline{K_t(\boldsymbol{r}+\tfrac{\boldsymbol{r}_1}{2},\boldsymbol{r}'+\tfrac{\boldsymbol{r}_2}{2})\, K_t^*(\boldsymbol{r}-\tfrac{\boldsymbol{r}_1}{2},\boldsymbol{r}'-\tfrac{\boldsymbol{r}_2}{2})}. \tag{15b}$$

Here the quantum propagator $K_t(\boldsymbol{r}_1,\boldsymbol{r}_2) = \langle \boldsymbol{r}_1|U(t)|\boldsymbol{r}_2\rangle$ is the probability amplitude to end up at point $\boldsymbol{r}_1$ at time t when starting at point $\boldsymbol{r}_2$ at time $t=0$. In Feynman's path description, K_t is expressed as a sum over all possible paths connecting $\boldsymbol{r}_2$ and $\boldsymbol{r}_1$. This assures that G_t indeed contains the non-local quantum interference that affects the density dynamics in phase space. It can be readily checked that G_t satisfies:

$$\lim_{t\to 0} G_t(\boldsymbol{r},\boldsymbol{k};\boldsymbol{r}',\boldsymbol{k}') = (2\pi)^d\, \delta(\boldsymbol{r}-\boldsymbol{r}')\, \delta(\boldsymbol{k}-\boldsymbol{k}') \tag{16a}$$

$$\int \frac{d\boldsymbol{r}d\boldsymbol{k}}{(2\pi)^d}\, G_t(\boldsymbol{r},\boldsymbol{k};\boldsymbol{r}',\boldsymbol{k}') = 1, \tag{16b}$$

where the latter merely expresses, as it should, conservation of the total density.

2.4 Disorder-averaged probability density

Using the previous results, it is easy to show that the average number density distribution is given by

$$p(\boldsymbol{r},t) = \int \frac{d\boldsymbol{r}'d\boldsymbol{k}'}{(2\pi)^d}\, F_t(\boldsymbol{r}-\boldsymbol{r}',\boldsymbol{k}')\, W_0(\boldsymbol{r}',\boldsymbol{k}'), \tag{17}$$

with a spatial propagation kernel given by

$$F_t(\boldsymbol{r}-\boldsymbol{r}',\boldsymbol{k}') = \int \frac{d\boldsymbol{k}}{(2\pi)^d}\, G_t(\boldsymbol{r},\boldsymbol{k};\boldsymbol{r}',\boldsymbol{k}'). \tag{18}$$

Taking advantage of the translation invariance, one can develop the intensity kernel into its Fourier components at fixed momentum $\boldsymbol{k}$,

$$\Phi(\omega,\boldsymbol{q},\boldsymbol{k}) = \int d\boldsymbol{r}dt\, e^{i(\omega t - \boldsymbol{q}\cdot\boldsymbol{r})}\, F_t(\boldsymbol{r},\boldsymbol{k}). \tag{19}$$

Probability conservation and linear response theory [9] imply that for long times and distances, i.e., small ω and q, the kernel takes the diffusive form

$$\Phi(\omega,\boldsymbol{q},\boldsymbol{k}) = \frac{1}{-i\omega + D(\omega,\boldsymbol{k})\, q^2} \tag{20}$$

featuring the ω-dependent diffusion constant $D(\omega,\boldsymbol{k})$ that can be calculated microscopically by quantum transport theory [9,18]. In this paper, we only consider situations where the disorder average restores translational and rotational symmetry, as exemplified by the potential correlator (2). This assumption implies in particular that the diffusion constant $D(\omega,\boldsymbol{k})$ must be a scalar and can only depend on $|\boldsymbol{k}| = k$. Before turning to the microscopic theory, we first explore which are the observable consequences of the diffusive form (20) in transport experiments with cold atoms.

2.5 Variance of the expanding cloud

The position variance of the expanding cloud of cold atoms in the speckle potential gives direct access to the diffusion

constant. Indeed, the variance of the expanding cloud is defined by $\Delta \boldsymbol{r}^2 = \langle \boldsymbol{r}^2 \rangle - \langle \boldsymbol{r} \rangle^2$ where $\langle ... \rangle$ denotes the average with respect to $p(\boldsymbol{r}, t)$. Using (17), (19), and (20) one finds:

$$\Delta \boldsymbol{r}^2(t) = \Delta \boldsymbol{r}_0^2 - 2d \int \frac{d\omega}{2\pi} \frac{\mathcal{D}(\omega)}{(\omega + i0)^2} \, e^{-i\omega t} \tag{21}$$

where $\Delta \boldsymbol{r}_0^2$ is the initial variance of the atomic cloud. The notation $\omega + i0$ indicates that the integration over frequency has to circumvent the pole at $\omega = 0$ from above in order to describe forward-time propagation. Here, the effective diffusion constant

$$\mathcal{D}(\omega) = \langle D(\omega, k) \rangle_{\pi_0} = \int \frac{d\boldsymbol{k}}{(2\pi)^d} \, \pi_0(\boldsymbol{k}) \, D(\omega, k) \tag{22}$$

is the k-dependent diffusion constant averaged over the initial momentum distribution $\pi_0(\boldsymbol{k})$.

2.6 Interaction-driven momentum distribution

We wish to calculate the average diffusion constant $\mathcal{D}(\omega)$ using the momentum distribution of an expanding Bose-Einstein condensate (BEC) released from an isotropic harmonic trapping potential with frequency Ω. Initially, the interacting condensate with chemical potential $\mu \gg \hbar\Omega$ is trapped in a Thomas-Fermi parabola with radius R determined by $\mu = \frac{1}{2} m \Omega^2 R^2$. When the harmonic trap is switched off, the expansion occurs in two steps. For small times $\Omega t \ll 1$, the repulsive interactions drive the expansion and the condensate acquires a dynamical phase. For long times $\Omega t \gg 1$, the density drops so much that the expansion becomes free and the condensate wavefunction takes the form [19]

$$\phi(\boldsymbol{r}, t) \propto \sqrt{1 - z^2} \, \Theta(1 - z) \, \exp(iuz^2), \tag{23}$$

with $z = r/(\sqrt{2} R \Omega t)$ and $u = 2\mu t/\hbar$. Since $\Omega t \gg 1$ and $\mu/(\hbar\Omega) \gg 1$, one can use a stationary-phase approximation with $u \gg 1$ to calculate the Fourier transform to the momentum domain, which is stationary:

$$\tilde{\phi}(\boldsymbol{k}) \propto \sqrt{1 - (k\xi)^2} \, \Theta(1 - k\xi) \tag{24}$$

here, $\xi = \hbar/\sqrt{4m\mu}$ is the healing length defined such that $\mu = \hbar^2/4m\xi^2$. Hence, the normalized momentum distribution $\pi_0(\boldsymbol{k}) = |\tilde{\phi}(\boldsymbol{k})|^2$ is given by

$$\pi_0(\boldsymbol{k}) = \frac{(2\pi\xi)^d}{S_d} \frac{d(d+2)}{2} \, (1 - (k\xi)^2) \, \Theta(1 - k\xi) \tag{25}$$

where S_d denotes the surface of the $(d-1)$-dimensional unit sphere ($S_1 = 2, S_2 = 2\pi, S_3 = 4\pi$). This distribution has again the form of an inverted parabola with an upper cut-off $k_{\max} = 1/\xi$ [12].

When the asymptotic regime of free expansion is reached, the speckle potential is switched on. The distribution $\pi_0(\boldsymbol{k})$ then constitutes the initial momentum distribution for the evolution of the condensate in the disordered potential.

3 Classical transport: the Boltzmann picture

In order to put the above results to work, let us first calculate the dynamics of particles in a disordered potential if all interference effects can be neglected. This is the realm of classical transport theory, whose origins date back to the Drude-Boltzmann theory of metals, more than one century ago [18,20,21], and that was later adapted to light propagation through interstellar atmospheres (radiative transfer theory) [22]. The basic physical ingredients of this description are (i) first to assume that any possible interference effects are washed out under disorder average (random-phase assumption) and (ii) second to devise a detailed-balance analysis of energy transfer in phase space (scattering, absorption, sources, etc). This powerful description leads to a physically very simple and appealing picture: sufficiently far from the boundaries and in the hydrodynamic regime of long times and large distances, transport is described by *diffusion*. Note that the description of transport in terms of a Boltzmann equation as such – and by its diffusive limit at long time and large distances – is *not* restricted to the weak scattering limit established in Section 2.2 above. However, it is in the weak-scattering regime that macroscopic quantities can be easily computed from the microscopic ones as will be shown in the following.

3.1 Boltzmann transport mean free path

When all interference corrections to the intensity kernel can be neglected (see Sect. 5 below for a more detailed derivation) one finds a finite diffusion constant in the stationary limit of frequency $\omega \to 0$ given by [9]

$$D_{\mathrm{B}}(k) = \frac{\hbar}{md} k \ell_{\mathrm{B}}(k) = \frac{v \ell_{\mathrm{B}}}{d} = \frac{\ell_{\mathrm{B}}^2}{\tau_{\mathrm{B}}}. \tag{26}$$

Note that this expression formally remains valid beyond the weak scattering limit, provided the full dispersion relation (instead of the free-particle expression $v = \hbar k/m$) is used for the average velocity. The Boltzmann transport mean-free path ℓ_{B} is the characteristic spatial scale beyond which memory of the initial direction is lost. It thus identifies with the average step of the random walk induced by the scattering processes. This classical transport mean-free path can be calculated both from the microscopic theory [9] and from a detailed-balance *Ansatz*, by an angular integral over the differential cross section of a single scattering event, weighted by the scattering anisotropy factor $(1 - \cos\theta)$:

$$\frac{1}{k\ell_{\mathrm{B}}} = \frac{\eta^2}{\kappa^{4-d}} \int \frac{d\Omega_d}{(2\pi)^{d-1}} (1 - \cos\theta) P\left(2\kappa \sin(\theta/2)\right), \tag{27}$$

here $\kappa = k\zeta$, $d\Omega_2 = d\theta$ in 2D (integration range from 0 to 2π) and $d\Omega_3 = 2\pi \sin\theta \, d\theta$ in 3D (integration range from 0 to π).

In the weak-scattering regime, the elastic scattering mean-free path ℓ_{s} is given by expression (27) with the

anisotropy factor replaced by 1. For the correlated potentials considered here (either the speckle or the Gaussian one), $\ell_{\rm B}$ is larger than ℓ_s, the two being asymptotically equal in the low-energy limit where scattering is isotropic, as shown in Figure 1.

An analytic expression for $\ell_{\rm B}$ is available in the small- and large-momentum limit [9] for the 2D optical speckle correlator (3) where $\zeta = \zeta_{\rm opt}$:

$$k\ell_{\rm B} = k\ell_{\rm s} \approx \frac{(k\zeta)^2}{4\pi\eta^2}, \qquad k\zeta \ll 1, \quad (28a)$$

$$k\ell_{\rm B} = \frac{15}{4}\,(k\zeta)^2\, k\ell_{\rm s} \approx \frac{45\pi(k\zeta)^5}{128\eta^2}, \qquad k\zeta \gg 1. \quad (28b)$$

For the Gaussian correlation (5b) with $\zeta = \zeta_{\rm gauss}$, one finds in 2D an analytical result valid for all momenta k,

$$\frac{1}{k\ell_{\rm B}} = \frac{2\pi\eta^2}{k^2\zeta^2} e^{-k^2\zeta^2}\left[I_0(k^2\zeta^2) - I_1(k^2\zeta^2)\right], \quad (29)$$

where I_ν is the modified Bessel function. This result has also been derived in [23] in a different context. In the low-energy limit $k\zeta \ll 1$ both optical speckle and Gaussian correlations result in the same expression

$$\frac{1}{k\ell_{\rm B}} = \frac{P(0)\eta^2}{k^2\zeta^2} = \frac{P(0)E_\Delta}{2E_k}, \quad (30)$$

just as substituting $P\,(2\kappa\sin(\theta/2)) \approx P(0)$ in (27) would have given. Hence $k\ell_{\rm B} \gg 1$ in the weak-disorder regime $E_k \gg E_\Delta$.

On the high-momentum side, it is important to note that contrary to the 1D case [5,12], in 2D the transport mean-free path $\ell_{\rm B}(k)$ is finite for all k-values, even though the potential correlator may have finite support, because even fast atoms can be deflected ever so slightly by a smooth random potential.

3.2 The Diffuson kernel

With the frequency-independent diffusion constant $D_{\rm B}(k)$, the intensity propagation kernel is easily calculated from (19) and (20) and reads

$$F_{\rm B}(r,k,t) = (4\pi D_{\rm B}(k)t)^{-d/2}\,\exp[-r^2/(4D_{\rm B}(k)t)]. \quad (31)$$

This Boltzmann kernel, known as the *diffuson* [21], obeys the diffusion equation:

$$\partial_t F_{\rm B} - D_{\rm B}\nabla^2 F_{\rm B} = \delta(\boldsymbol{r})\delta(t). \quad (32)$$

The diffuson obviously fulfills probability conservation. Interestingly enough, it also boils down to $\delta(\boldsymbol{r})$ when $t \to 0$ even though its expression is in principle only valid at large enough times. The range of validity of this diffusive description is then expressed as $r \gg \ell_{\rm B}$ and $t \gg \tau_{\rm B}$ in terms of the Boltzmann transport time $\tau_{\rm B} = \ell_{\rm B}^2/D_{\rm B}$. With the interaction-driven momentum distribution (24), this will occur for the whole distribution as soon as

$$\frac{4\mu t}{\hbar d} \gg k_{\max}\ell_{\rm B}, \quad \frac{r}{\xi} \gg k_{\max}\ell_{\max} \quad (33)$$

where $\ell_{\max} = \ell_{\rm B}(k_{\max} = 1/\xi)$.

Since diffusion in phase space occurs with a momentum-dependent diffusion constant, the average probability density $p(r,t)$ itself does not obey a diffusion equation. But going back to (17), we note that for times large enough, the spatial width of the diffuson will always be much larger than the spatial width of W_0. This implies that, in the long-time limit, the probability density is well approximated by the momentum-distribution average

$$p(r,t) \approx \langle F_{\rm B}(r,k,t)\rangle_{\pi_0}. \quad (34)$$

Finally, with the frequency-independent diffusion constant $D_{\rm B}(k)$, one finds that the variance (21) of the expanding cloud increases as expected linearly in time,

$$\Delta\boldsymbol{r}^2(t) = \Delta\boldsymbol{r}_0^2 + 2d\mathcal{D}_B t, \quad (35)$$

with the momentum-averaged diffusion constant analogous to (22),

$$\mathcal{D}_B = \langle D_{\rm B}(k)\rangle_{\pi_0}. \quad (36)$$

This average over the inverted-parabola distribution (25). can be easily evaluated numerically for any of the mean-free paths (27) – (30) above. An analytical result is available in the low-energy limit:

$$\mathcal{D}_B = \frac{D_{\rm B}(k_{\max})}{3} = \frac{1}{3}\,\frac{\hbar}{2m}\,\frac{2E_{\max}}{P(0)E_\Delta} \quad (37)$$

where $E_{\max} = 2\mu$ in terms of the initial chemical potential. This is a good approximation only if the momentum dispersion is so small that $k_{\max}\zeta = \zeta/\xi \ll 1$, i.e., in the limit where already the initial condensate is weakly interacting.

4 Coherent transport and localization

The ensemble average over static disorder alone cannot wipe out interference effects, and Boltzmann's description does not adequately describe phase-coherent propagation. Indeed, the constructive interference between amplitudes counter-propagating along loop-like paths survives the disorder average and increases the particle's probability to return to its starting point. This increased tendency to stay behind translates into a reduced diffusion constant, an effect called weak localization (WL) [18,21,24]. Under suitable conditions, this can even completely inhibit diffusion, a phenomenon known as strong (or Anderson) localization (SL). It is rigorously proven that transport in 1D bulk samples is always suppressed by strong localization, and on the basis of the single-parameter scaling theory this remains valid also in 2D, whereas in 3D localization occurs only when $k\ell_{\rm B} \lesssim 1$ (Ioffe-Regel criterion); further details can be found in the recommendable review [3].

4.1 "Loop-renormalized" diffusion constant

Phase-coherent bulk transport in the weak localization regime $k\ell_{\rm B} \gg 1$ can be described by a diagrammatic perturbation theory, developed by Vollhardt and

Wölfle [10,18]. When weak-localization interference effects are self-consistently taken into account, the Boltzmann diffusion constant $D_{\rm B}(k)$ is renormalized into an interference-reduced diffusion constant $D(\omega,k)$ solving

$$\frac{1}{D(\omega,k)} = \frac{1}{D_{\rm B}(k)} + \frac{A_d(k)}{D_{\rm B}(k)} C(\omega,k) \tag{38}$$

where $A_d(k) = (2\pi)^d \hbar/(m\pi S_d k^{d-2})$. This formula features the "return probability" $C(\omega,k)$, given by

$$C(\omega,k) = \int \frac{d\boldsymbol{q}}{(2\pi)^d} \frac{1}{-i\omega + D(\omega,k)\, q^2} \tag{39}$$

in the diffusive regime. A mean-field like, self-consistent description is obtained because the corrected diffusion constant $D(\omega,k)$ enters the diffusive propagator under the integral. The implicit equation for $D(\omega,k)$ can be conveniently rewritten as

$$D_{\rm B}(k) = D(\omega,k) + \frac{\hbar}{\pi m k^{d-2}} \int \frac{q^{d-1} dq}{q^2 - i\omega/D(\omega,k)}. \tag{40}$$

In our previous articles [8,9], we have studied directly the stationary regime at $\omega = 0$. Presently, we will explore the consequences of the finite-frequency approach, which turns out to be quite powerful.

The formal integral for the return probability (40) may present divergences, either infrared (for small q) or ultraviolet (for large q), that have to be regularized by suitable cutoffs. Working at finite frequency ω has the advantage that the integral stays finite as $q \to 0$, so there is no need for introducing a special infrared cutoff.

However, the return probability in 2D displays a logarithmic ultraviolet divergence ($q \to \infty$). We regularise it by introducing an appropriate upper bound $q_{\rm max}$, defined as the minimal distance beyond which interference can play a role. Since the return probability is evaluated in the diffusive regime, we have chosen this minimal distance to be the Boltzmann transport mean free path and accordingly imposed $1/\ell_{\rm B}$ as the upper bound. Please note that there is no need to dress also this ultraviolet cutoff by localization corrections: during the short time required to scatter through small loops, corresponding to $\omega \approx \tau_B^{-1}$, the interference corrections will be shown to be negligible just below.

4.2 Weak and strong localization in 2D

Solving now (40) for $d = 2$, we obtain the functional dependence of $X = D(\omega,k)/D_{\rm B}(k)$ on ω at fixed k through the implicit equation [25]:

$$-i\omega\tau_{\rm B} = \frac{X}{\exp[\pi k \ell_{\rm B}(1-X)] - 1}. \tag{41}$$

In the weakly disordered regime $k\ell_{\rm B} \gg 1$, it is advisable to rewrite this transcendental equation as

$$X = 1 - \frac{1}{\pi k \ell_{\rm B}} \log\left[1 - \frac{X}{i\omega\tau_{\rm B}}\right], \tag{42}$$

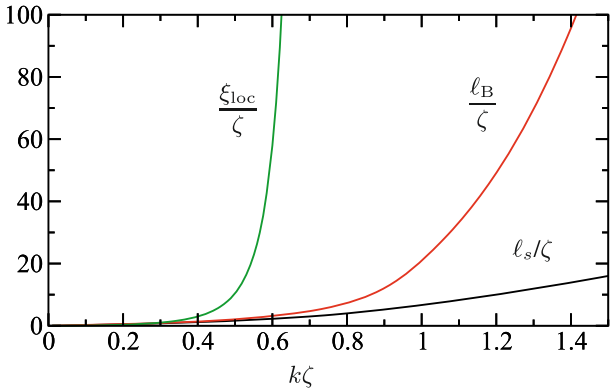

Fig. 1. Scattering mean free path ℓ_s, Boltzmann transport mean free path $\ell_{\rm B}$ (Eq. (27)) and localization length $\xi_{\rm loc}$ (Eq. (44)) as a function of the atomic wave vector k, all measured in units of the correlation length $\zeta = \zeta_{\rm opt}$ of a 2D speckle potential. The disorder strength is $\eta = V/E_\zeta = 0.2$. Note the extremely rapid increase of the localization length, a characteristic feature of 2D localization.

which gives as perturbative solution the celebrated weak-localization correction [26,27]

$$\frac{D_{\rm WL}(\omega,k)}{D_{\rm B}(k)} = 1 - \frac{1}{\pi k \ell_{\rm B}} \log\left[1 - \frac{1}{i\omega\tau_{\rm B}}\right]. \tag{43}$$

In the frequency range $\omega\tau_{\rm B} \approx 1$ of small diffusive loops, this correction is negligible. This means that the diffusion of a particle starts off with a classical Boltzmann random walk and is consistent with the choice of the unrenormalized ultraviolett cutoff $q_{\rm max} = 1/\ell_{\rm B}$ discussed in the previous subsection.

At intermediate times $\omega\tau_{\rm B} \ll 1$ the weak localization corrections described by (43) kick in. This expression is valid as long as the correction is not too large, i.e., for $\omega\tau_{\rm B} > (\ell_{\rm B}/\xi_{\rm loc})^2$ in terms of the new (and important) spatial scale

$$\xi_{\rm loc}(k) = \ell_{\rm B}(k)\sqrt{\exp[\pi k \ell_{\rm B}(k)] - 1} \approx \ell_{\rm B} e^{\pi k \ell_{\rm B}/2} \tag{44}$$

whose significance will become clearer in a moment. For even smaller frequencies $\omega\tau_{\rm B} \ll (\ell_{\rm B}/\xi_{\rm loc})^2$ the solution of (41) crosses over to the asymptotic behaviour

$$D(\omega,k) \approx -i\omega\xi_{\rm loc}^2(k). \tag{45}$$

This linear dependence on frequency with $\lim_{\omega\to 0} D(\omega,k) = 0$ implies that the diffusion stops in the long-time limit. The intensity propagation kernel (19) calculated with the asymptotic solution (45) is stationary:

$$F_\infty(r,k) = \int \frac{d\boldsymbol{q}}{(2\pi)^2} \frac{e^{i\boldsymbol{q}\cdot\boldsymbol{r}}}{1 + q^2\xi_{\rm loc}^2} = \frac{K_0(r/\xi_{\rm loc})}{2\pi\xi_{\rm loc}^2} \tag{46}$$

where K_0 is a modified Bessel function [28]. The asymptotics for large distances $K_0(x) = \sqrt{\pi/2x}\,{\rm e}^{-x}$ shows an exponential decay, and we see that $\xi_{\rm loc}(k)$ is the localization length.

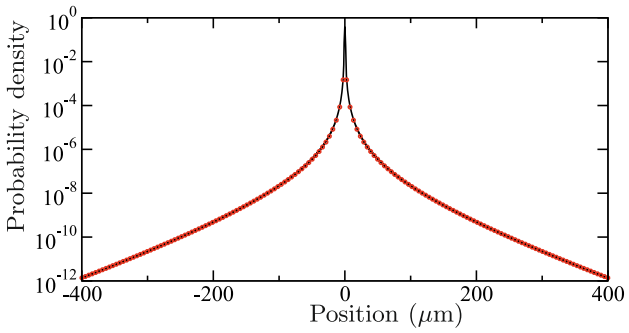

Fig. 2. Solid black line: stationary spatial probability density (47) of a BEC wavepacket initially in the Thomas-Fermi regime at disorder strength $\eta = 0.2$ and $k_{\max}\zeta = 0.65$. Note the logarithmic scale and the fact that most of the wavepacket remains well localized near the initial position, an effect of the small-k-components of the wavepacket. Only in the far tails where the density is extremely low one observes exponential localization with localization length $\xi_{\rm loc}(k_{\max}) \approx 48\,\mu$m. The full shape of the wavepacket is well described by $\exp[-r/\xi_{\rm loc}(k_{\max})]/r^{5/2}$ (red circles).

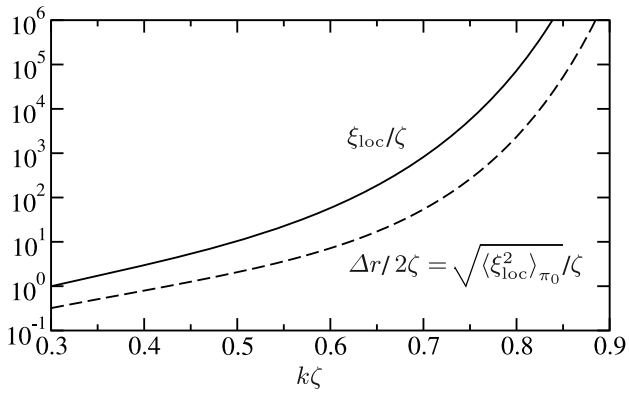

Fig. 3. Solid curve: localization length $\xi_{\rm loc}$ (Eq. (44)) as a function of the atomic wave vector k for $\eta = 0.2$, both in units of the 2D-speckle correlation length ζ. Dashed line: stationary rms size $\Delta r/2$ of the wavepacket (Eq. (48)) resulting from the expansion of an initial Thomas-Fermi wavepacket with maximum momentum $k_{\max} = k$. As a result of the average, various shorter localization lengths contribute and the resulting final size of the wavepacket is significantly smaller than in the monochromatic case with the corresponding $k = k_{\max}$. Note, however, that both curves display a similar rapid increase with k.

As noted in Section 3.1 above, in 2D the transport mean-free path $\ell_{\rm B}(k)$ is finite for all k-values. Consequently, the localization length $\xi_{\rm loc}(k)$ as given by (44) is also finite, and there is exponential localization for all k-components in the initial momentum distribution $\pi_0(\boldsymbol{k})$. This implies that a wavepacket will follow a diffusive behaviour at short time, but the dynamics will slow down and finally freeze. The resulting stationary probability distribution depends on the initial state. Provided that the initial spatial size of the wavepacket is small compared to the effective width $\Delta r(k) \equiv \xi_{\rm loc}(k)$ of the propagation kernel (for the k values populated in the initial wavepacket), the limit distribution reads

$$\lim_{t\to\infty} p(r,t) \approx \left\langle \frac{K_0(r/\xi_{\rm loc}(k))}{2\pi\xi^2_{\rm loc}(k)} \right\rangle_{\pi_0} . \qquad (47)$$

This final density distribution is shown in Figure 2 for the typical values $\eta = 0.2$ and $k_{\max}\zeta = 0.65$ used throughout this paper. Obviously, the shape near the center is not purely exponential. Only quite far in the tails is the wavepacket component at $k_{\max}$ dominant, leading to exponential localization with localization length $\xi_{\rm loc}(k_{\max}) \approx 48\,\mu$m. Except very close to the origin, the density distribution is quite well described by $\exp[-r/\xi_{\rm loc}(k_{\max})]/r^{5/2}$ as obtained by using the asymptotic behaviour of K_0 in equation (47).

This behaviour in 2D can be compared to other dimensions. In 1D, and still within the Born approximation, two regimes have to be distinguished. In case the highest momentum lies still inside the support of the speckle two-point correlator, all k-components are exponentially localized, and an asymptotic behaviour $\exp(-|z|/\xi_{\rm loc}(k_{\max}))/|z|^{7/2}$ is predicted [12]. In case the highest momenta are beyond the support of the two-point correlation, then a regime can be reached with an effective algebraic density decay as $|z|^{-2}$; these predictions have been recently confirmed by experiments [5]. In 3D, averaging over the same momentum distribution leads to a $|r|^{-4}$ algebraic decay, without any exponential envelope. This is due to atoms with momenta close to the mobility edge, at least for the limiting case of uncorrelated Gaussian disorder [29]. Thus, only in two dimensions do we have the favourable situation where the density profile always shows an exponential localization. This is because the two dimensional localization length is always finite for all k-components for correlated disorder even within the Born approximation.

Solving next for the variance (21) we get:

$$\lim_{t\to\infty} \Delta\boldsymbol{r}^2(t) = \Delta\boldsymbol{r}_0^2 + 2d\left\langle\xi^2_{\rm loc}(k)\right\rangle_{\pi_0} \qquad (48)$$

when the initial dispersion $\Delta\boldsymbol{r}_0^2$ can be neglected, the spatial variance will be given by the momentum-average of the squared localization length plotted in Figure 3. This is the essence of strong localization: Transport starts in the Boltzmann regime and, as time increases, the diffusive dynamics gets slowed down by interference effects. Finally the dynamics freezes in the stationary limit and 2D transport always reaches the localized regime within a bulk system in the absence of phase-breaking mechanisms. The time scale for the complete crossover from the diffusive to the stationary localized distribution shown in Figure 2 is given by the localization time $\tau_{\rm loc}(k_{\max}) = \xi^2_{\rm loc}(k_{\max})/D_{\rm B}(k_{\max})$ for the fastest atoms with momentum $k_{\max}$. Of course, some components of the atomic cloud (the ones with lower momenta) will localize earlier and on a shorter spatial scale, resulting in a strongly peaked probability density, see Figure 2.

5 Quantum diffusion with limited phase coherence

Since 2D localization relies on interfering amplitudes over loops of arbitrary size and since the bulk localization length $\xi_{\rm loc}$ increases exponentially fast with $k\ell_{\rm B}$, one must imperatively discuss spatial or temporal factors limiting the interference effects. An important limitation is due to dephasing, and another obvious limitation is the finite size of the sample. Within the framework established so far, we are able to take into account both limitations. First we consider a bulk system with dephasing, turning to limited system size in the following Section 6.

5.1 Dephasing processes

Perfect phase coherence is of course an idealization, and in real systems interference effects are killed by dephasing processes at some rate $\gamma_\phi = \tau_\phi^{-1}$. This means that the contribution of long diffusion loops to the interference-renormalized diffusion constant is suppressed.

To incorporate dephasing processes in the self-consistent theory, we implement the simple prescription $\omega \mapsto \omega + i/\tau_\phi$ in (39). This replacement can be shown to be exact within linear response theory for a rather large class of different systems with microscopic dephasing sources, such as electrons with spin-flip scattering by magnetic impurities or photons being scattered by atoms with a degenerate dipole transition [30]. Also mobile impurity atoms in a two-species experiment can be a source of dephasing randomness [31], and in the limiting case of slowly moving impurities an effective dephasing time is obtained that leads to the same qualitative consequences as the above substitution [32].

It is important to stress here that the intensity propagation kernel (20) keeps unchanged under dephasing, i.e., there ω is not to be shifted by i/τ_ϕ. This fact outlines an important difference between dephasing processes and absorption. Dephasing kills interference, hereby affecting the self-consistent diffusion constant given by (40), but conserves particle number. Uniform absorption would cause particle losses at some constant rate $\gamma_a = \tau_a^{-1}$. It would not affect the relative phase between interfering amplitudes, but would damp their contribution as the loop size increases, thereby hindering the cumulative strength of interference effects. In the present paper, we consider conservative dynamics and therefore do not need to discuss absorption, which could be conveniently incorporated in the theory by the substitution $\omega \mapsto \omega + i/\tau_a$ both in (20) and in (39).

In the present context of atoms in optical potentials, we consider that the main source of decoherence for the atom dynamics is the spontaneous emission of photons from the speckle field [8,9]. These spontaneous emission processes occur at a rate

$$\frac{1}{\tau_\phi} = \frac{V\Gamma}{\hbar|\delta|} \tag{49}$$

where Γ is the natural linewidth of the excited atomic state and δ is the detuning with respect to the atomic transition frequency.

If the average time between successive spontaneous emission events is of the order of – or even shorter than – the Boltzmann transport time, $\tau_\phi \lesssim \tau_{\rm B}$, then this intense dephasing will be shown below to result in purely classical transport already discussed in Section 3. If on the contrary $\tau_\phi \gg \tau_{\rm B}$, then the regime of coherent diffusive transport is reached. Since $\tau_\phi/\tau_{\rm B}$ scales as $V|\delta|/\Gamma$, this can be always achieved at constant potential height provided the detuning $|\delta|/\Gamma$ is sufficiently large.

5.2 Weak localization and residual diffusion

After the replacement $\omega \to \omega + i/\tau_\phi$ in the self-consistent implicit equation (42), we can now discuss its solution along the lines of Section 4.2. Let us consider the stationary limit $\omega \to 0$. The stationary diffusion constant solves now the self-consistent equation

$$\frac{D(k)}{D_{\rm B}(k)} = 1 - \frac{1}{\pi k\ell_{\rm B}} \log\left[1 + \frac{\tau_\phi D(k)}{\tau_{\rm B} D_{\rm B}(k)}\right]. \tag{50}$$

In the case of intense dephasing $\tau_\phi \lesssim \tau_{\rm B}$, we get $D \to D_{\rm B}$, a result easy to understand: coherent effects are scrambled at such a high rate that Boltzmann diffusion is never affected by interference. The dynamics thus stays entirely classical, and the results of Section 3 apply. Of course, the random momentum recoil transferred to the atoms by rapid spontaneous emission of photons induces already an atomic diffusion by itself [33], but here we assume that this effect is negligible compared to the disorder-induced diffusion under study.

More interesting is now the regime of phase-coherent transport $\tau_\phi \gg \tau_{\rm B}$. As in Section 4.2, the short-time dynamics $\omega\tau_{\rm B} \sim 1$ is again dominated by the classical Boltzmann diffusion. However, the limit $\omega \to 0$ does not lead anymore to strong localization in the strict sense. Instead, in the stationary limit, the residual dynamics stays diffusive. In the case of moderate dephasing, i.e. $\tau_\phi \ll \tau_{\rm loc} = \xi_{\rm loc}^2/D_{\rm B}$, from (50) one finds the weak-localization correction to the diffusion constant in the form

$$D_{\rm WL}(k) = D_{\rm B}(k) - \frac{\hbar}{2\pi m} \ln\left(1 + \frac{\tau_\phi}{\tau_{\rm B}}\right). \tag{51}$$

In the last case of very weak dephasing, $\tau_\phi \gg \tau_{\rm loc}$, the residual diffusion constant is

$$D(k) \approx \frac{\xi_{\rm loc}^2(k)}{\tau_\phi} = D_{\rm B}(k)\frac{\tau_{\rm loc}(k)}{\tau_\phi}. \tag{52}$$

We can picture this regime by saying that coherent effects tend to localize the particle but phase-breaking mechanisms impose a residual slow diffusion with $D \ll D_{\rm B}$: the particle propagates coherently over a relatively long time and thus localizes in time $\tau_{\rm loc}$ on a scale $\xi_{\rm loc}$ until a phase-breaking event occurs (typically every τ_ϕ), resetting the diffusive Boltzmann dynamics followed by localization after another $\tau_{\rm loc}$, etc.

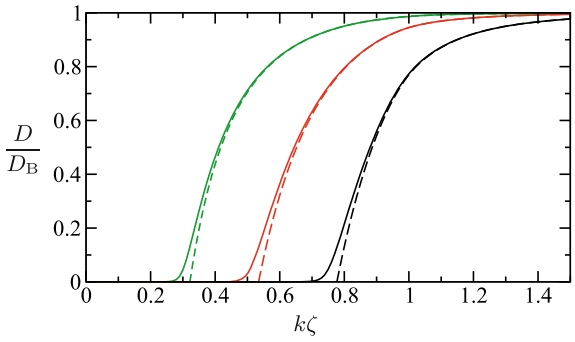

Fig. 4. Solid lines: diffusion constant $D/D_{\rm B}$ given by equation (50) as a function of $k\zeta$ for increasing disorder strength (from left to right) η =0.05 (green), 0.1 (red), 0.2 (black). Decoherence is driven here by spontaneous emission induced by the light-shift speckle field itself, cf. [8,9]. The speckle detuning is chosen at $\delta = 3.29 \times 10^7 \Gamma$, where Γ is the width of the atomic excited state, realizing highly phase-coherent propagation with $\tau_\phi/\tau_{\rm B} \sim 10^7$. The crossover from weak localization at high k to residual diffusion at small k is rather sharp. Dashed curves: corresponding plots of the ratio $D_{\rm WL}/D_{\rm B}$ as given by (51). The localization onset at $k_{\rm c}$ where $D_{\rm WL} = 0$ gives a reasonably good approximation to the crossover.

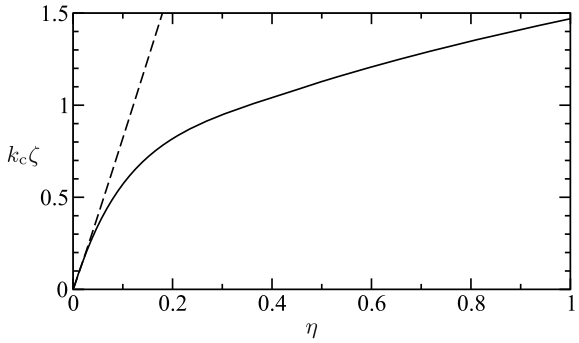

Fig. 5. Critical wavenumber $k_{\rm c}\zeta$ (defining the effective onset of strong localization) as a function of the disorder strength η in the optical speckle field with correlation (3) and detuning $\delta = 3.29 \times 10^7 \Gamma$. The dashed line is the low-energy behaviour (54).

5.3 Localization onset in presence of dephasing

Let us now examine more closely the crossover from weak to strong localization as a function of relevant parameters. Figure 4 shows a plot of $D/D_{\rm B}$ solving (50) (together with the weak localization prediction (51)) as a function of $k\zeta$ for different values of disorder strength η. The laser detuning from the atomic resonance is held fixed at $\delta = 3.29 \times 10^7 \Gamma$. For $k\zeta < 1$, the low-energy limit (28a) then permits to estimate the effective dephasing rate as $\tau_\phi/\tau_{\rm B} = 2\pi\eta|\delta|/\Gamma$, which varies slightly with η from curve to curve but is exceedingly large (of the order of 10^7) in all cases.

Clearly, the curves show a sharp crossover between the weak localization regime at large momentum and residual diffusion at small momentum. The crossover between these two regimes can be conveniently defined through the condition $\tau_\phi = \tau_{\rm loc}$. Recasting the weak-localization corrections (51) in the form

$$\frac{D_{\rm WL}}{D_{\rm B}} = \frac{1}{\pi k \ell_{\rm B}} \ln\left(\frac{\tau_{\rm B} + \tau_{\rm loc}}{\tau_{\rm B} + \tau_\phi}\right) \qquad (53)$$

One immediately sees that the crossover condition $\tau_\phi = \tau_{\rm loc}$ is reached at the point where the weakly localized diffusion constant would vanish: $D_{\rm WL} = 0$.

Solving for this condition defines an effective mobility edge $k_{\rm c}$ in momentum space as a function of the disorder parameters such as its strength $\eta = V/E_\zeta$. Figure 5 shows a numerical plot of $k_{\rm c}$ as a function of η as obtained for the 2D speckle correlator (3) in the case of spontaneous emission at detuning $\delta = 3.29 \times 10^7 \Gamma$. At low energy, one can use (28a) to obtain:

$$k_{\rm c}\zeta = 2\eta \sqrt{\ln\left(1 + 2\pi\eta|\delta|/\Gamma\right)}, \quad (k\zeta \ll 1). \qquad (54)$$

This low-energy asymptotics is also shown in Figure 5. Note that the weak-disorder condition $\eta \ll k_{\rm c}\zeta$ is well satisfied for $\eta \ll 1$.

From a practical point of view, one can thus say that an effective strong localization regime is reached when only residual diffusion with $D \ll D_{\rm B}$ takes place. Consequently, one can earmark all momentum states with $k < k_{\rm c}$ as "localized" and all states with $k > k_{\rm c}$ as "extended". The localized fraction of atoms in this sense is

$$p_{\rm loc} = \int_{k \le k_{\rm c}} \frac{d\boldsymbol{k}}{(2\pi)^d}\, \pi_0(\boldsymbol{k}) = \beta^2(2 - \beta^2) \qquad (55)$$

where $\beta = \min(1, k_{\rm c}/k_{\rm max})$. Not surprisingly, localizing a large fraction of atoms requires that almost all momenta present in the initial distribution are below the effective mobility edge.

6 Finite-size systems

The impact of long diffusion loops is also limited by spatial boundaries in finite-size systems. As justified in [34], a correct way to deal with finite-size systems is to introduce a *space-dependent* renormalized diffusion constant. A detailed calculation also requires to know which boundary conditions are imposed at the edges of the system. Obviously, periodic or fixed boundary conditions (Dirichlet or Neumann) impose a discrete energy spectrum while open boundary conditions give a continuous spectrum and thus the impossibility of true localization (in the strict mathematical sense) at infinite time, because of leakage at the edges.

A much simpler recipe is the replacement $q^2 \to q^2 + 1/L^2$ in the integrand of the return probability (40) (an equivalent alternative is to use $1/L$ as an infrared cutoff for the q-integral), thereby suppressing the contribution of long loops. Without a precise prescription of what happens at the boundaries (absorption, reflection with a phase shift, periodic boundary conditions, etc.), this is the simplest approach. As we will see in the following, it leads nevertheless to physically reasonable

results in the localized regime. Of course, the system size must not be too small for diffusion to take place, and one should have $L \gg \ell_B$.

In order to implement this simple approach, one may still work with the complex-frequency method used in the previous section and use the formal prescription $\omega \to \omega + i/\tau_L$ with $\tau_L = L^2/D$, a form which is suggestive of the average time it would take an atom with effective diffusion constant $D(\omega, k)$ to reach the boundary. This cutoff time is obtained from the Thouless time $\tau_{Th} = L^2/D_B$ if one replaces the bare diffusion constant D_B by the self-consistently renormalized D. Note that although $\tau_L = L^2/D$ formally acquires an imaginary part if $D(\omega, k)$ does, the replacement in (40) still provides a real momentum replacement $q^2 \to q^2 + 1/L^2$ because $D(\omega, k)$ is divided out.

In principle, one should also use the (non-self-consistent) replacement $\omega \to \omega + i/\tau_{Th}$ in the intensity propagator (20). Like uniform absorption, this leakage would lead to a global exponential damping of the probability density, also known as the fundamental Holstein mode of the system [35]. In the localized regime where the system size is larger than the bulk localization length, $L \gg \xi_{loc}(k)$, this damping (whose precise effect would again depend on the boundary conditions) is expected to be small and can be neglected.

6.1 Onset of localization in a finite-size system

We now briefly discuss the case of a finite-size system in the absence of dephasing mechanisms ($\tau_\phi \to \infty$). Using the finite-size replacement $\omega \to \omega + i/\tau_L$ in the self-consistent equation (42) one determines the stationary diffusion constant in the limit $\omega \to 0$, which turns out to be a non-zero real quantity when $\xi_{loc}(k) > L$:

$$D(k) = \frac{\hbar}{2\pi m} \ln\left[\frac{\ell_B^2(k) + \xi_{loc}^2(k)}{\ell_B^2(k) + L^2}\right]. \qquad (56)$$

As this is precisely the regime where boundary conditions must be carefully specified, this result must be taken with a grain of salt, and only gives an indication of how much the classical transport is slowed down by interference effects.

The situation is more interesting below the critical momentum k_c defined by the condition $\xi_{loc}(k_c) = L$. There, the stationary diffusion constant vanishes, implying localization, and the asymptotic low-frequency behaviour is:

$$D(\omega, k) \approx -i\omega \xi_{loc}'^2(k). \qquad (57)$$

with a modified localization length [9]:

$$\frac{1}{\xi_{loc}'^2(k)} = \frac{1}{\xi_{loc}^2(k)} - \frac{1}{L^2}. \qquad (58)$$

This expression says that cutting off very long loops in a finite system slightly increases the localization length. Note that this correction is algebraic in L/ξ_{loc} while absorption at the boundary is expected to be exponentially small. Les us repeat that this simple approach is valid only if the system size is larger than the bulk localization length. When this condition is violated, a space-dependent diffusion constant and proper boundary conditions must be considered.

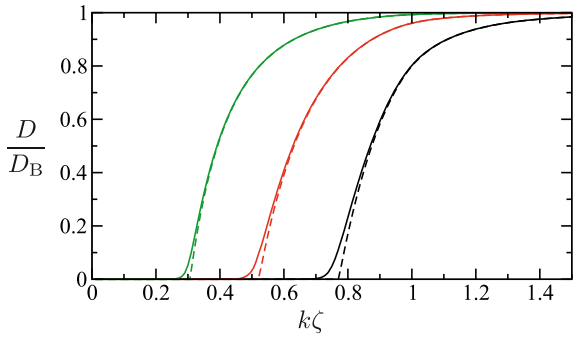

Fig. 6. Reduced diffusion constant $D(k)/D_B(k)$ as a function of reduced atomic wave number $k\zeta$ for increasing disorder strength (from left to right) η =0.05 (green), 0.1 (red), 0.2 (black). Dashed line: only the finite size $L = 4$ mm of the system is taken into account. The onset of localization with vanishing D happens when the localization length of the infinite system equals the system size. Solid line: when dephasing effects such as spontaneous emission (detuning $\delta = 3.29 \times 10^7 \Gamma$) are taken into account, the transition is smoothed.

6.2 Localization in a finite-size system with dephasing

We account for the possibility of transport occurring inside a finite domain while suffering from dephasing by summing the respective rates, $\tau_0^{-1} = \tau_L^{-1} + \tau_\phi^{-1}$, a prescription reminiscent of the Matthiessen rule [20]. If one prefers to reason in terms of length scales, one may define the effective (complex) phase-coherence length $\ell_\phi = \sqrt{D\tau_\phi}$ and use $L_0^{-1} = [L^{-2} + \ell_\phi^{-2}]^{1/2}$ as momentum cutoff through $q^2 \to q^2 + L_0^{-2}$. Since the complex diffusion constant is divided out, note again that this prescription is just equivalent to use real cutoffs through $-i\omega + Dq^2 \to -i\omega + \tau_\phi^{-1} + D(q^2 + L^{-2})$.

If both finite size and dephasing are taken into account, there is no strict onset for localization, but, as in the situation with pure dephasing, an effective threshold below which residual diffusion is tiny, $D \ll D_B$. Figure 6 shows the ratio of the diffusion constant – obtained by solving the self-consistent equation (42) – to the Boltzmann diffusion constant, when the finite size of the system is taken into account, and when dephasing effects are included. Comparison with Figure 4 shows that the effect of the finite system size in this case is rather small.

7 Localization in experiments

7.1 Effect of the initial momentum distribution

Knowing the diffusion constant $D(k)$ for each momentum k, the average diffusion constant (22) can be computed by

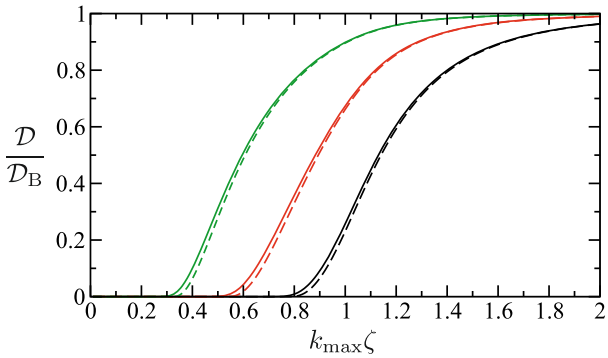

Fig. 7. Solid curves: ratio of momentum-averaged diffusion constants $\mathcal{D}/\mathcal{D}_B$ as a function of $k_{max}\zeta$ of an expanding BEC with momentum distribution (25) for increasing disorder strength (from left to right) $\eta = 0.05$ (green), 0.1 (red), 0.2 (black). The speckle correlation function is given by (3), the detuning has been fixed to $\delta = 3.29 \times 10^7\, \Gamma$. Dashed curves: $\mathcal{D}_{WL}/\mathcal{D}_B$ obtained from the weak-localization prescription (51) and (59).

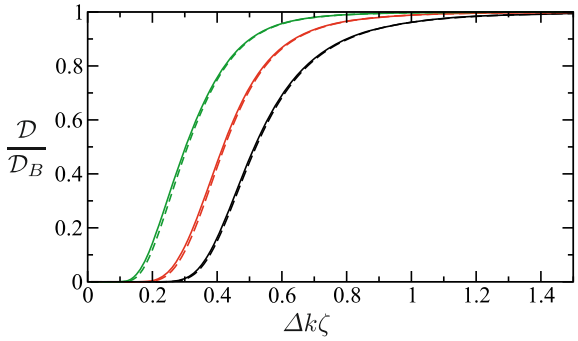

Fig. 8. Same as in Figure 7, but for a Gaussian momentum distribution with dispersion Δk.

integration over the Thomas-Fermi momentum distribution (25) of an expanding BEC. One can use either the self-consistent diffusion constant $D(k)$ or its approximation in the weak localization regime $D_{WL}(k)$. In the latter case, the integral must be cut below k_c in order to avoid counting an unphysical negative D_{WL}:

$$\mathcal{D}_{WL} = \int_{k>k_c} \frac{d\boldsymbol{k}}{(2\pi)^d}\, \pi_0(\boldsymbol{k})\, D_{WL}(k). \qquad (59)$$

Figure 7 shows the ratio $\mathcal{D}/\mathcal{D}_B$ as a function of $k_{max}\zeta$ for different values of η and the 2D speckle correlation (3). A value of $\mathcal{D}/\mathcal{D}_B$ close to 1 means that quantum corrections to transport are difficult to observe. Conversely they become very strong when this value approaches zero. Atoms are then practically completely localized. The threshold in k to observe localization increases with η, or equivalently, with k_c. We find again the criterion $k_{max} \sim k_c$ to observe "strong localization" rather unambiguously.

In [13], a Gaussian initial wavepacket is discussed instead of a Thomas-Fermi distribution, leading to a Gaussian momentum distribution centered at $k = 0$ with dispersion Δk. Figure 8 gives our results for the ratio $\mathcal{D}/\mathcal{D}_B$ as a function of $\Delta k\zeta$ for different values of η. Compared to Figure 7, there are no qualitative changes and no big quantitative changes. Hence the conclusions keep the same.

7.2 Experimental realizability

In order to estimate the orders of magnitude expected for a realistic 2D experiment, we will use the various experimental parameters of the quasi-1D Orsay experiment [5]. There, a BEC condensate of Rb^{87} atoms ($m \approx 1.44 \times 10^{-25}$ kg) is produced with a healing length $\xi \approx 0.40\,\mu$m. The condensate evolves in an optical speckle with correlation length $\zeta \approx 0.26\,\mu$m such that $k_{max}\zeta = \zeta/\xi \approx 0.65$. The optical speckle size $L \approx 4$ mm is far-detuned from the Rb transition frequency by $\delta/\Gamma \approx 3.29 \times 10^7$. The speckle fluctuation strength can be adjusted by varying the laser power, up to $\eta \approx 0.046$. For reasons explained below, we performed calculations for $\eta = 0.05, 0.1$ and 0.2. Since $\eta/k_{max}\zeta$ is then at most 0.3 (and therefore sufficiently less than 1), we can use the weak-disorder results, keeping in mind that exact numerical values can differ from the ones computed in lowest-order perturbation theory.

Compared to the 1D situation, the main difficulty in 2D is to reach a sufficiently short transport mean free path ℓ_B. Indeed, the exponential dependence of the localization length ξ_{loc} with ℓ_B – see equation (44) – implies that $k\ell_B$ must not be much larger than unity, so that $k\xi_{loc}$ itself can be at most of the order of few hundreds or thousands, meaning ξ_{loc} smaller or comparable to 1 mm. Then, the Boltzmann diffusion constant, equation (26), will be of the order of a few $\hbar/m$, that is a few $10^{-9}\,m^2\,s^{-1}$. As the lifetime of an ultra-cold atomic gas is typically limited to a few seconds, it is clear that the maximum diffusive expansion of the gas will be limited to a few hundred μm. This in turn implies that localization by interference effects will be observed only if the localization length is decreased to a sufficiently small value, of the order of a fraction of a mm. This is very different from the 1D situation, where localization can be observed even for a large transport mean free path (between 50 μm and 2 mm in [5]) and a large Boltzmann diffusion constant. A fortunate consequence is that the size of the speckle optical potential can be limited to a fraction of mm, making it possible to focus the laser power on a smaller area, such that values of η up to 0.2 should be reachable.

With these parameter values, the effective mobility edge is predicted to be at $k_c\zeta \approx 0.345$, 0.571 and 0.818 for $\eta = 0.05$, 0.1 and 0.2, respectively. We thus predict that about 48%, 95% and 100% of the atoms will be localized, respectively. Evidence of the 2D localized regime should thus be easily observable.

With $\eta = 0.2$, the maximum localization length (for atoms with $k = k_{max}$) is about 48 μm, and the localization time around 2.6 s. Loss of coherence by spontaneous emission should occur at a very small rate, of the order of $\tau_\phi^{-1} \approx 6.7 \times 10^{-5}\,s^{-1}$, leading to a tiny residual diffusion constant, of the order of 10^{-4} times the Boltzmann diffusion constant. These very favorable numbers are due to

the choice of a far off-resonance laser beam to create the optical potential. A different technical choice for the laser beam could of course lead to a different situation.

In conclusion, these estimates show that strong localization of matter waves in 2D speckle potentials is within experimental reach.

8 Conclusion

We have studied quantum diffusion of matter waves propagating in 2D optical speckle potentials within the framework of a self-consistent localization theory. We have consistently incorporated the effect of dephasing mechanisms and system boundaries. We have calculated the average probability density $p(\boldsymbol{r}, t)$ of matter waves propagating in a disordered potential for any initial Wigner phase-space distribution. This quantity allows to calculate the variance of the expanding cloud. We have shown that dephasing processes prevent true localization from taking place and induce a residual diffusion in the long-time limit. In certain regimes of parameters, the resulting stationary diffusion constant is so small that, for all practical purposes, one can define a localization onset by the momentum where the bulk weakly localized diffusion constant vanishes. This mobility edge then separates "localized" states from "extended" ones, allowing for a practical definition of the localized fraction of atoms. These quantities serve as experimental parameters to study weak and strong localization from a practical point of view.

We have specialized our results to the case of an interaction-driven BEC expanding in the presence of the disordered optical potential and to the case of a Gaussian momentum distribution. In any case strong localization can only be achieved for cold enough atoms. Taking state-of-the-art figures we have shown that Anderson localization of matter waves in 2D optical speckle potentials should be observable in near-future experiments.

The authors would like to thank Guillaume Labeyrie for raising this subject and for many helpful discussions about this work. This work was supported by the DAAD, the BFHZ-CCUFP and the Marie Curie program (contract number HPMT-2000-00102) at Laboratoire Kastler Brossel (Université Pierre et Marie Curie/École Normale Supérieure, UMR 8552 du CNRS). RK would like to thank Professor B.-G. Englert and the Quantum Information Lab at the National University of Singapore for their kind hospitality (A*STAR Temasek Grant 012-104-0040).

References

1. M. Lewenstein, A. Sanpera, V. Ahufinger, B. Damski, A. Sen, U. Sen, Adv. Phys. **56**, 243 (2007)
2. P.W. Anderson, Phys. Rev. Lett. **109**, 1492 (1958)
3. B.V. Tiggelen, in *Diffuse Waves in Complex Media*, edited by J.P. Fouque (Kluwer, 1999), pp. 1–60
4. B. Kramer, A. MacKinnon, Rep. Progr. Phys. **56**, 1469 (1993)
5. J. Billy, V. Josse, Z. Zuo, A. Bernard, B. Hambrecht, P. Lugan, D. Clément, L. Sanchez-Palencia, P. Bouyer, A. Aspect, Nature **453**, 891 (2008)
6. G. Roati, C. D'Errico, L. Fallani, M. Fattori, C. Fort, M. Zaccanti, G. Modugno, M. Modugno, M. Inguscio, Nature **453**, 895 (2008)
7. E. Abrahams, P.W. Anderson, D.C. Licciardello, T.V. Ramakrishnan, Phys. Rev. Lett. **42**, 673 (1979)
8. R.C. Kuhn, C. Miniatura, D. Delande, O. Sigwarth, C.A. Müller, Phys. Rev. Lett. **95**, 250403 (2005)
9. R. Kuhn, O. Sigwarth, C. Miniatura, D. Delande, C.A. Müller, New J. Phys. **9**, 161 (2007)
10. D. Vollhardt, P. Wölfle, Phys. Rev. B **22**, 4666 (1980)
11. B. Shapiro, Phys. Rev. B **25**, 4266 (1982)
12. L. Sanchez-Palencia, D. Clément, P. Lugan, P. Bouyer, G.V. Shlyapnikov, A. Aspect, Phys. Rev. Lett. **98**, 210401 (2007)
13. B. Shapiro, Phys. Rev. Lett. **99**, 060602 (2007)
14. D. Clément, A.F. Varón, J.A. Retter, L. Sanchez-Palencia, A. Aspect, P. Bouyer, New J. Phys. **8**, 165 (2006)
15. J.W. Goodman, in *Laser speckle and related phenomena*, edited by J.C. Dainty (Springer-Verlag, 1975)
16. M. Hartung, T. Wellens, C.A. Müller, K. Richter, P. Schlagheck, Phys. Rev. Lett. **101**, 020603 (2008)
17. M. Hillery, R.F. O'Connell, M.O. Scully, E.P. Wigner, Phys. Rep. **106**, 121 (1984)
18. J. Rammer, *Quantum Transport Theory* (Perseus Books, Reading, Mass., 1998)
19. Y. Kagan, E.L. Surkov, G.V. Shlyapnikov, Phys. Rev. A **54**, R1753 (1996)
20. N. Ashcroft, D. Mermin, *Solid State Physics* (Saunders College, Philadelphia, 1976)
21. E. Akkermans, G. Montambaux, *Mesoscopic physics of electrons and photons* (Cambridge University Press, Cambridge, 2007)
22. S. Chandrasekhar, *Radiative Transfer* (Dover Publications, New York, 1960)
23. V.M. Apalkov, M.E. Raikh, B. Shapiro, J. Opt. Soc. Am. B **21**, 132 (2004)
24. E. Akkermans, G. Montambaux, J.L. Pichard, J. Zinn-Justin, Mesoscopic Quantum Physics, *Proceedings of the Les Houches Summer School Session LX1* (Elsevier Science, Amsterdam, 1995)
25. O.I. Lobkis, R.L. Weaver, Phys. Rev. E **71**, 011112 (2005)
26. L. Gor'kov, A. Larkin, D. Khmel'nitskiĭ, Pis'ma Zh. Eksp. Teor. Fiz. **30**, 248 (1979) [JETP Lett. **30**, 228 (1979)]
27. G. Bergmann, Phys. Rep. **107**, 1 (1984)
28. M. Abramowitz, I. Stegun, *Handbook of mathematical functions with formulas, graphs, and mathematical table* (Dover Publications, New York, 1972)
29. S.E. Skipetrov, A. Minguzzi, B.A. Van Tiggelen, B. Shapiro, Phys. Rev. Lett. **100**, 165301 (2008)
30. C.A. Müller, C. Miniatura, E. Akkermans, G. Montambaux, J. Phys. A: Math. Gen. **38**, 7807 (2005)
31. S. Ospelkaus, C. Ospelkaus, O. Wille, M. Succo, P. Ernst, K. Sengstock, K. Bongs, Phys. Rev. Lett. **96**, 180403 (2006)
32. E. Kogan, Eur. Phys. J. B **61**, 181 (2008)
33. G. Grynberg, C. Robilliard, Phys. Rep. **355**, 335 (2001)
34. N. Cherroret, S.E. Skipetrov, Phys. Rev. E **77**, 046608 (2008)
35. G. Labeyrie, E. Vaujour, C.A. Müller, D. Delande, C. Miniatura, D. Wilkowski, R. Kaiser Phys. Rev. Lett. **91**, 223904 (2003)